Microstrip EHF Butler Matrix Design and Realization

Jean-Sébastien Néron and Gilles-Y. Delisle

This paper describes the design and realization of an extra high frequency band 8 × 8 microstrip Butler matrix. Operation at 36 GHz is achieved with a frequency bandwidth exceeding 400 MHz. The circuit is implemented on a bi-layer microstrip structure using conventional manufacturing processes. This planar implementation of a Butler matrix is a key component of a switched beam smart antenna with printed antenna elements integrated on-board. Conception details, simulation results, and measurements are also given for the components (hybrid couplers, cross-couplers, and vertical inter-connections) used to implement the matrix.

Keywords: Butler matrix, microstrip, beam forming.

I. Introduction

Scientific studies [1], [2] based on indoor channel measurement campaigns have shown that highly directive antennas used at both the transmitter and receiver of a communication system can reduce considerably the delay spread of the signal reaching the receiver while at the same time improve the signal gain. Electronically-steered phased arrays are well known for their ability to generate a directive beam according to a given control signal and may be a possible multipath mitigation solution. One way to implement this electronic scanning is by using electronically controlled phase shifters. Another approach would be to generate a set of predefined beams and select among them the beam with satisfying properties. A subset of these beams (or all of them) with proper weighting can also be combined in such a way that a desired array response is obtained.

The latter alternative requires a beamforming network that transforms the signal from the N antenna elements to a predefined set of M beams. The Butler matrix [3] is such a network, as shown in Fig. 1, and is realized with hybrid couplers, phase shifters, and crossovers, which makes it a totally passive circuit. This matrix generates a set of N orthogonal beams from the N antenna elements of an equi-spaced linear array.

This paper details the realization of an 8 × 8 Butler matrix and its constituting components. In order to minimize the space occupied by the microwave circuit and also to ease its production, a planar implementation using microstrip transmission lines has been chosen. These lines are especially interesting when connections with other components are required such as antennas and connectors. There are only a few similar realizations in the literature [4]-[6] and none of these are in the extra high frequency (EHF) band (most of them are for frequencies below or around 5 GHz).

Manuscript received Feb. 01, 2005; revised Nov. 09, 2005.

The material in this work was presented in part at CIC 2004, Seoul, Korea, Oct. 2004.

Jean-Sébastien Néron (phone: +1 418 656 2131, email: neron@gel.ulaval.ca) is with the Department of Electrical and Computer Engineering, Laval University, Québec, Canada.

Gilles-Y. Delisle (email: gilles.delisle@iitelecom.com) is with N.A., International Institute of Telecommunications, Montréal, Canada.

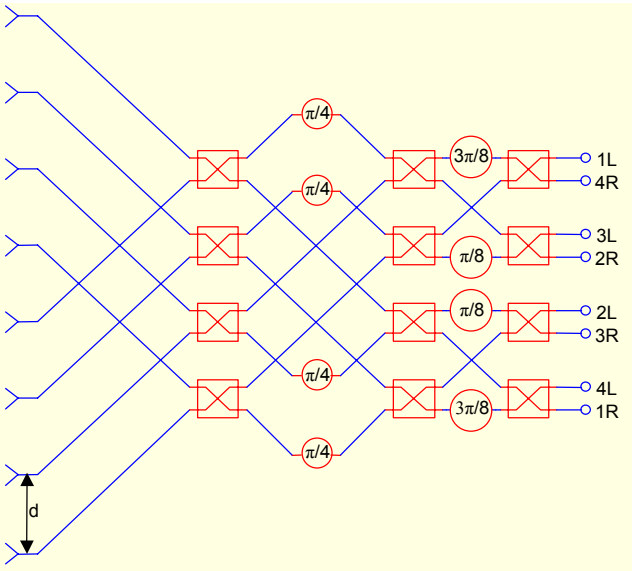

Fig. 1. The 8 × 8 Butler matrix fed by a linear array of equi-spaced antenna elements. The 4-port devices in red are hybrid couplers and the circular devices (also in red) are fixed phase shifts.

II. Analysis and Design

1. The Butler Matrix

The N × N Butler matrix creates a set of N orthogonal beams in space by processing the signal from the N antenna elements of an equi-spaced linear array. These beams are pointing in direction θ governed by the following equation [7]:

$$\sin\theta_i = \pm\frac{i\lambda}{2Nd}, \quad i = 1, 3, 5, \ldots, (N-1). \tag{1}$$

The corresponding inter-element phase shift with spacing $d = \lambda/2$ is

$$\alpha_i = \beta d \sin\theta_i = i\frac{\pi}{N}, \tag{2}$$

where $\beta = \frac{2\pi}{\lambda}$ is the wave number.

The realization of an 8 × 8 Butler matrix requires twelve quadrature hybrids and involves fourteen line crossings. This high number of crossings, as well as the relatively high circuit density, makes a planar realization on a single layer impractical, which is why a two-layer implementation has been chosen here.

2. Microstrip Implementation

One way to minimize line crossings is to subdivide the circuit in multiple layers. By splitting the circuit on two layers, the number of line crossings is reduced from fourteen to four and thereby decreases significantly the per layer circuit density for a given surface. This reduction of the part count per layer implies an inherent reduction in coupling from element to element (since they are less closely placed), and thus an improvement of the overall performance is obtained.

A. Substrate Selection and Transmission Lines

The realization is based on a superposition of two Rogers RT/Duroid 5880 substrates (ε_r=2.2, tanδ=0.0009, and h=254 μm) as shown in Fig. 2. These layers of substrates and conductors are held together by an RO3001 bonding film (ε_r=2.28, tanδ=0.003, and h=76.2 μm). Copper metallization for the three conductive layers (Cond, Slot/Gnd, and Cond2) is 17.5 μm thick.

Substrate selection has been motivated first by the necessity of antenna realization on the same board as the feed network. A low permittivity is essential for good radiation efficiency and satisfying the bandwidth of the antennas at the cost of an increased radiation of the feed network.

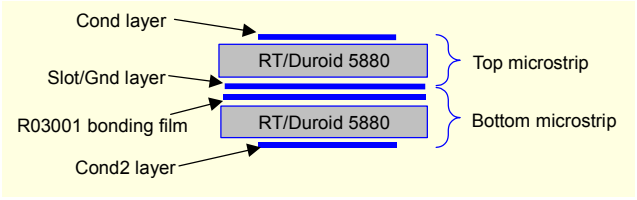

Fig. 2. The bi-layer microstrip assembly used for this realization.

A second requirement influencing substrate selection is the physical dimensions of transmission lines and the losses. A good substrate has low dielectric losses, and these losses are directly related to its loss tangent. Moreover, since the manufacturing of this circuit is made using the conventional photolithographic process, special care should be taken to make sure that the artwork dimensions are such that the etching error is not affecting too much the performance. We can't expect tolerances better than ±35 μm using standard PCB manufacturing facilities, and this can lead to considerable deviations from simulations to experiments.

An initial investigation of the line dimensions and parameters for a few scenarios was made, and results are summarized in Table 1. These results are derived from numerical simulations and optimization using the method of moments (MOM) as implemented by the commercial software Agilent Momentum and its optimization engine. Empirical models are a good starting point for the dimensions of the lines, but there is a discrepancy between our optimized results and the empirical ones, which can be explained by the fact that these models are not taking into account higher order

Table 1. Line characteristics for various substrates at 36 GHz with a 17.5 μm thick copper metallization.

Parameter	Symbol	Unit	Case 1	Case 2	Case 3	Case 4	Case 5
Substrate			RT/Duroid 5880	RT/Duroid 5880	RT/Duroid 5880	RT/Duroid 6006	RT/Duroid 6006
Relative permittivity	ε_r		2.2	2.2	2.2	6.15	6.15
Loss tangent	tanδ		0.0009	0.0009	0.0009	0.0027	0.0027
Substrate height	h	μm	254	254	127	254	254
Line impedance	Z_0	Ω	100	50	50	100	50
Wavelength	λ	mm	6.213	6	6.032	4.09	3.84
Width	W	μm	239	794	400	64.5	393
Losses (per wavelength)		dB	0.1	0.08	0.13	0.21	0.11

phenomenas encountered at our design frequency. The final choice of transmission lines and substrate for this work corresponds to case 1 of the table.

B. Quadrature Hybrid

Quadrature hybrids or hybrid couplers are well known devices used for their ability to generate signals 90 degrees out of phase at its outputs. An analysis of the quadrature hybrid implemented using transmission lines as shown in Fig. 3 can be carried out by the even-odd mode decomposition as proposed by [8]. Following this development, the analytical *S* parameters of this four-port network as in [9] are

$$S = \frac{-1}{\sqrt{2}}\begin{bmatrix} 0 & j & 1 & 0 \\ j & 0 & 0 & 1 \\ 1 & 0 & 0 & j \\ 0 & 1 & j & 0 \end{bmatrix}. \tag{3}$$

The power applied at a port is evenly distributed between the ports located on the opposite side of the coupler. There is a 90 degree phase difference between these two ports; the port closer to the input port is leading in phase by 90 degrees. The port located on the same side as the input port is isolated since there is no power reaching it.

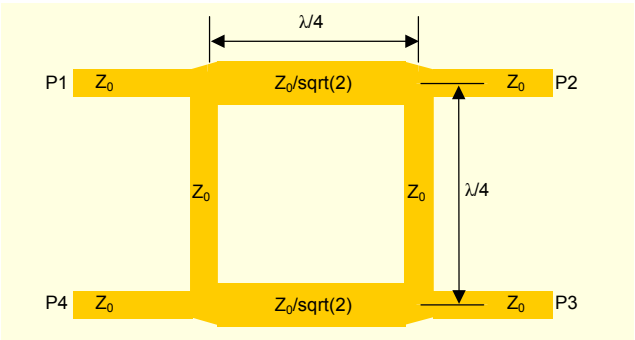

Fig. 3. The quadrature hybrid built around transmission lines.

C. Cross-coupler

These devices, also known as 0 dB couplers, are an efficient means of crossing two transmission lines with a minimal coupling between them. Referring to Fig. 4, it can be observed that the planar implementation is made here as a cascade of two hybrid couplers (with slight modifications on line widths).

Once again, an even-odd mode analysis can be applied here, and extending the approach given by [9] for the quadrature hybrid yields the following *S* parameters:

$$S = \begin{bmatrix} 0 & 0 & j & 0 \\ 0 & 0 & 0 & j \\ j & 0 & 0 & 0 \\ 0 & j & 0 & 0 \end{bmatrix}. \tag{4}$$

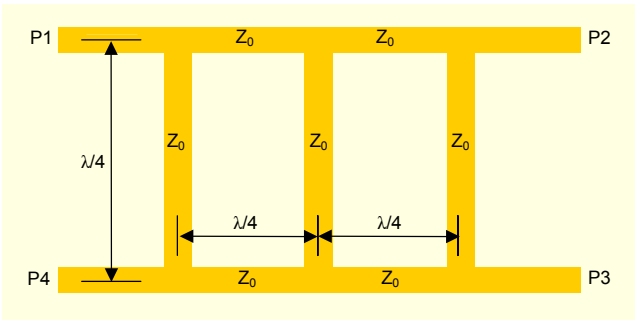

Fig. 4. The cross-coupler also known as a 0 dB coupler.

D. Vertical Interconnection

One drawback of using multiple layers is the fact that the necessity to pass signals between them is introduced. At lower frequencies, vias are commonly used, and their reliability as well as their performance is more than satisfying. However, as the frequency increases, this mean of signal transmission between layers requires proper alignment and dimensioning, which makes it a critical aspect of manufacturing.

The vertical interconnection is used here to transmit a signal

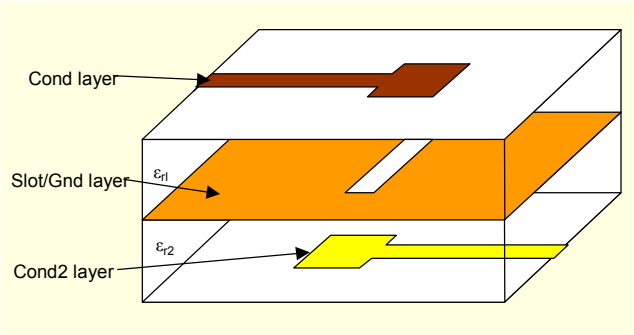

Fig. 5. The vertical interconnection between layers.

from one layer to the other by an electromagnetic coupling only. There is no DC path between the 2 layers since they are AC-coupled only, and this coupling is optimized for a particular frequency band. Figure 5 illustrates the concept.

A signal arriving on the upper transmission line (from the left) eventually reaches the end of this transmission line. The discontinuity created here radiates energy that is mostly coupled to the bottom line by the opening in the ground plane (some power may be radiated). The following aspects must be considered to achieve an optimal coupling between layers as well as a good matching of the transition:

- A proper positioning of the line ends relative to the slot center
- A proper dimensioning of the serial stub added at the end of the transmission lines is necessary
- The design of the slot in the ground plane: many shapes are possible (circular, bowtie, rectangular, and so on), and the dimensions should be carefully optimized
- Orientation of the lines over the slot.

For a better understanding of the complex interaction between the lines and the slot, a full-wave numerical simulation is essential. A lot of interesting works aiming to characterize these transitions have been published [10]-[13].

III. Simulations and Optimization

To better characterize the circuit, full-wave numerical simulations were performed using MOM by way of Agilent Momentum. This method of simulation offers a good modeling of arbitrary shapes, and it has been validated prior to the design of microwave components such as antennas and others.

1. Quadrature Hybrid

This coupler has been implemented in the layout environment of the Agilent ADS software suite. A first guess for proper dimensioning has been made using the design steps enumerated earlier in this paper. The simulated results were suboptimal, since our analytical model assumes perfect transmission lines and no coupling. Optimization was performed on this first attempt by allowing line lengths to vary. The desired performance was achieved with the dimensions as shown in Fig. 6. Some results are also given in Fig. 7.

As expected, the phase difference between port 3 and port 2 is 90 degrees. Insertion loss over the desired bandwidth of 400 MHz is around 0.4 dB for each branch, which is typical for this type of transmission medium at these frequencies.

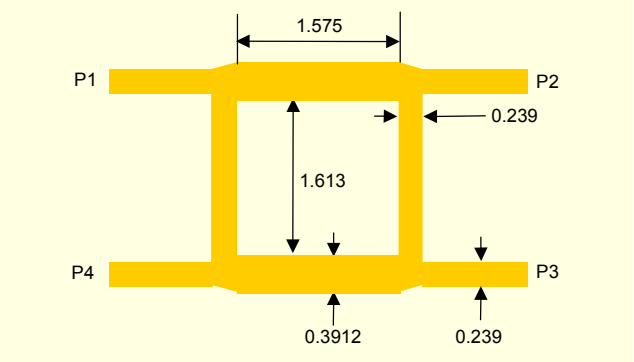

Fig. 6. The optimized quadrature hybrid (dimensions in mm).

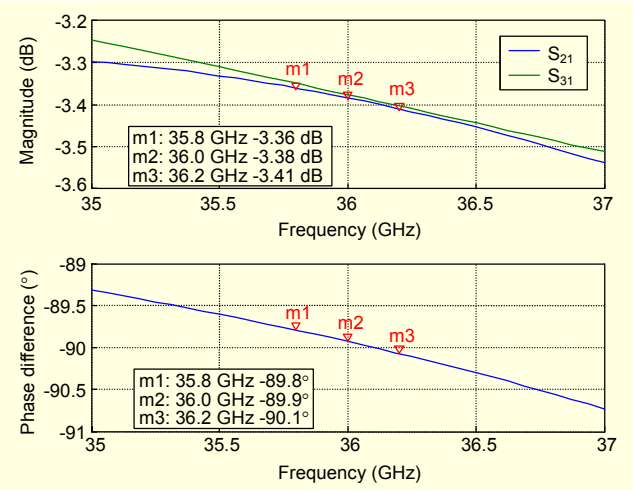

Fig. 7. Simulated S_{21} and S_{31} magnitudes for the quadrature hybrid and phase difference between in-phase and quadrature ports.

2. Cross-coupler

In the same way, the cross-coupler has been optimized, as the dimensions in Fig. 8 show, and the results are given in Fig. 9. The insertion loss for the coupled port is around 0.3 dB, while isolation is close to -30 dB for the frequency band of interest. This level of insertion loss, which is comparable to the performance of the quadrature hybrid, of course cannot be neglected.

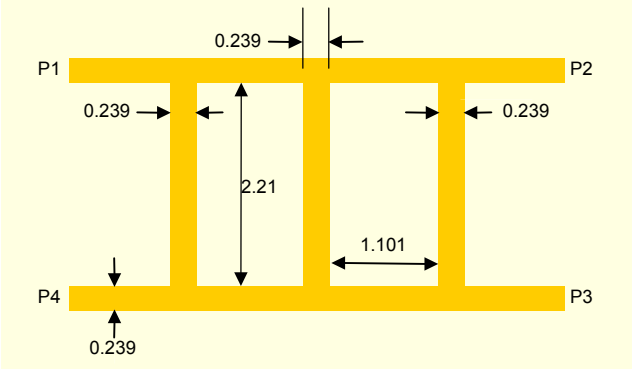

Fig. 8. The optimized cross-coupler (dimensions in mm).

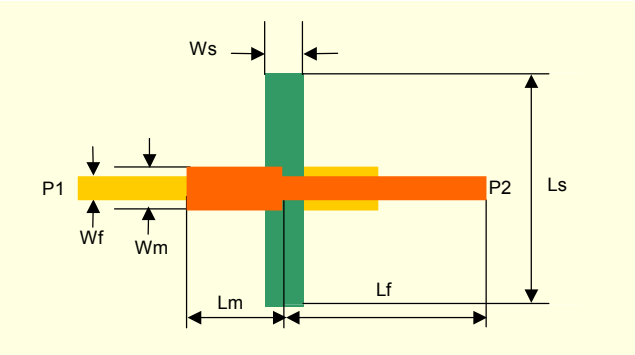

Fig. 10. The optimized vertical interconnection: dimensions in mm are Wf = 0.239, Lf = 2, Wm = 0.468 , Lm = 0.939, Ws = 0.35, and Ls = 2.432.

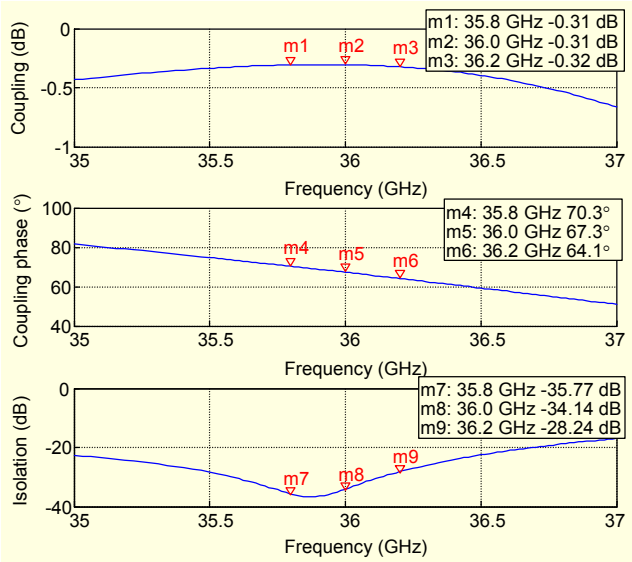

Fig. 9. Simulated insertion loss and isolation for the cross-coupler.

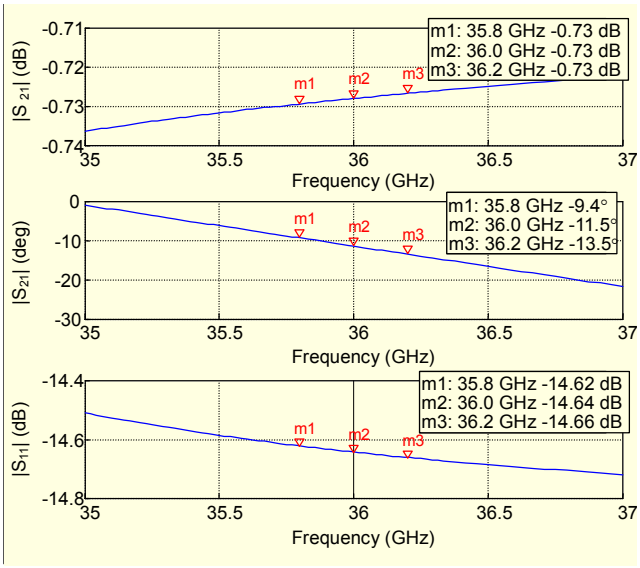

Fig. 11. Simulation results of the optimized vertical interconnection.

3. Vertical Interconnection

The vertical interconnection has been implemented using two conductive layers (orange and yellow) and a slot layer (green). This latter layer is implemented as a slot in an infinite ground plane, which makes the computation of the MOM solution for the opening only. Simulation results reveal an almost constant performance over the 400 MHz bandwidth centered on 36 GHz, and insertion losses are 0.73 dB.

4. The Butler Matrix

The physical implementation of the matrix is made of twelve cross-couplers, twelve quadrature hybrids, and four vertical interconnections as shown in Fig. 13. In theory, only four cross-couplers are required, but additional ones were also added on paths with no crossing in order to make all branches

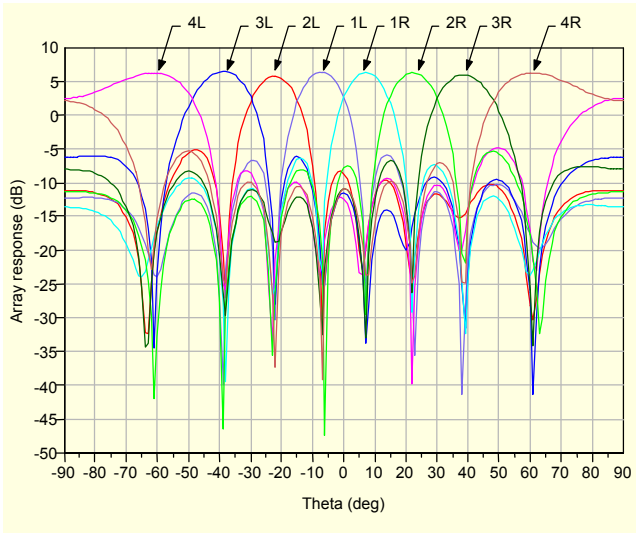

Fig. 12. Array radiation patterns with a linear array of equi-spaced isotropic antenna elements (no coupling considered).

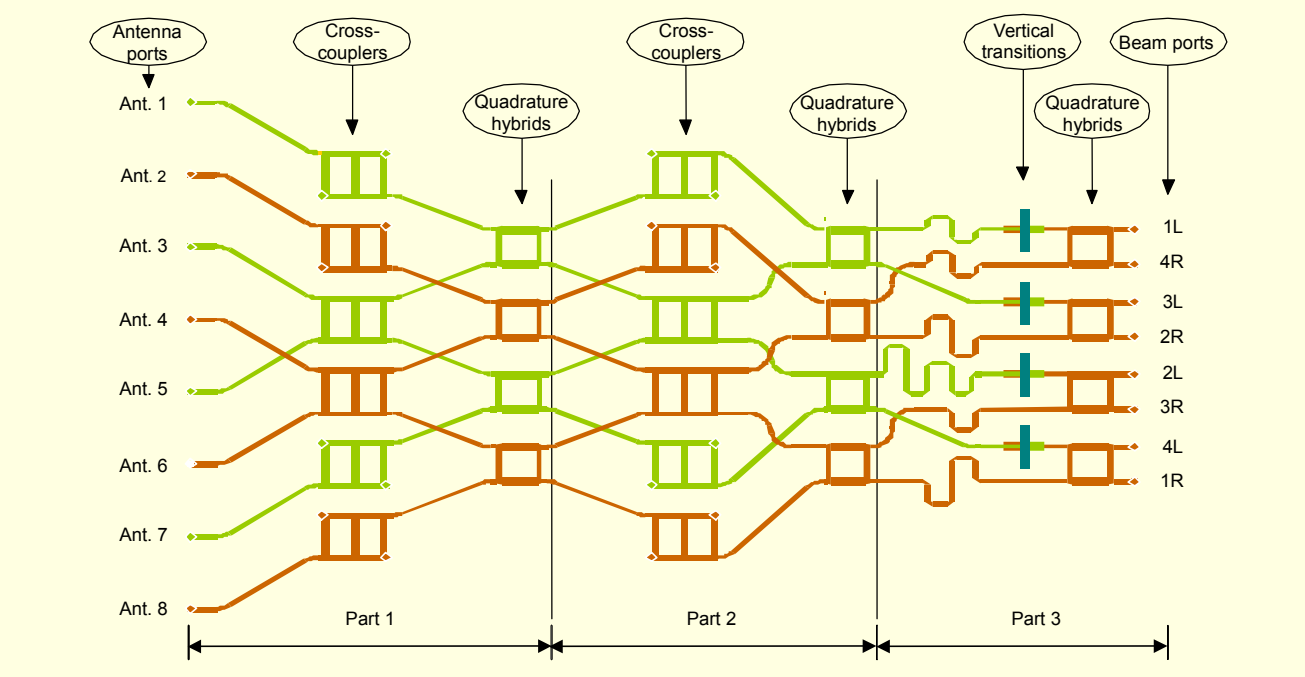

Fig. 13. The complete Butler matrix as realized (top layer in orange, bottom layer in yellow, and slot layer in green).

of the network similar in terms of phase shift and insertion loss. Since isolation of the cross-coupler is high enough, no line terminations were added on unused ports.

The required phase shifts (ϕ_0= 67.5°, 45°, and 22.5°), as shown in Fig. 1, are implemented using delay lines that introduce the required phase shift at the center frequency f_0 of 36 GHz. A little deviation from the ideal phase shift is observed at the extremities of the operational bandwidth and can be calculated as follows (assuming no dispersion in the microstrip lines over the frequency range of interest):

$$\Delta\phi = \phi_0 \frac{\Delta f}{f_0}, \tag{5}$$

where $\Delta f = f - f_0$. The largest phase error is ±0.375° and occurs at the ends of the band (for f=36.2 GHz and 35.8 GHz).

The complete circuit has been simulated using MOM, and since such a large layout means many unknowns to solve for, the simulation has been subdivided into more tractable parts as shown in Fig. 13. The simulated performance is close to the expectations: there is no deviation of the beam pointing direction $\theta_{\max}$ and losses are lowering the gain $G(\theta_{\max})$ of the array by 3.6 dB for the worst case. There is some degradation of the sidelobe level (SLL), which is caused by phase errors and amplitude unbalance between the ports. The asymmetry introduced by the vertical interconnections between layers is certainly affecting performance since they should have been lossless in theory.

These results are for a linear array of isotropic antenna elements evenly distributed with a spacing of half a wavelength between them. In order to compare simulations with theoretical results and for the sake of simplicity, coupling was not considered. Practical antenna elements have their specific radiation pattern, which differs from the isotropic ones, and coupling between antennas of the array may be severe for close spacing, as is the case here.

IV. Realization

The matrix has been realized and tested. Pictures of the realized components as well as experimental data are given in this section. The matrix and its individual components (except vertical interconnection, which has been tested on an Anritsu Universal Test Fixture) were mounted on an aluminum support allowing connector mounting and providing rigidity to the structure. To ensure good ground continuity between the connectors and the ground layer of the PCBs, silver filled epoxy has been used to bond the circuit to the aluminum support.

To make the measurements possible, 2.92 mm connectors were added to the devices. All the measurements were performed on an Agilent 8722ES network analyzer using TRL (thru-reflect-line) calibration on the substrate in order to remove connectors and cable influences.

1. Butler Matrix

Figure 14 illustrates the 8 × 8 Butler matrix as realized

showing equal-length transmission lines added in order to link connectors to the circuit. Also shown on the left of the circuit are the additional vertical transitions used to pass the signal from the bottom layer to the top layer, making connection to external circuits possible. The layout dimensions excluding connectors and the linking transmission lines are 46 mm × 30 mm, which makes this realization relatively compact.

Measurement of this type of device requires proper termination of unused ports (testing of the two-port scattering parameters in this case necessitates fourteen loads). Another approach would be to investigate the performance of the whole matrix with antennas connected directly to antenna ports, and thus lowering the fourteen termination-loads requirement at the expense of a more complicated circuit and making *S* parameter measurements impractical.

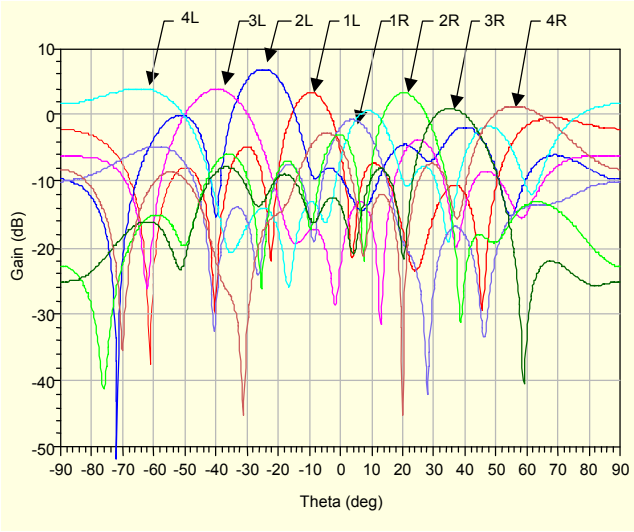

Fig. 14. Measured array radiation patterns as generated by the Butler matrix with equi-spaced (d=λ/2) isotropic antenna elements.

2. Quadrature Hybrid and Cross-coupler

The realized couplers were tested individually (quadrature hybrid is shown in Fig. 17). The cross-coupler was first tested (on the same fixture as the hybrid coupler) and its feeding transmission lines properly de-embedded using the numerically simulated scattering parameters of these lines. The performance in terms of coupling is -0.46 dB at 36 GHz which is 0.15 dB lower than predicted by simulations. The phase of the measured coupling coefficient is 52.2 degrees at 36 GHz, which is 15 degrees lower than predicted. The isolation is -24.07 dB at 36 GHz and is 10 dB lower than expected.

Since we did many connector/fixture tests with the hybrid coupler, the only remaining prototype got damaged at port 1, which implied a transmission line rework (using silver filled epoxy). The obtained results were absolutely not relevant, and unfortunately there are no measurement results available at this time for this component.

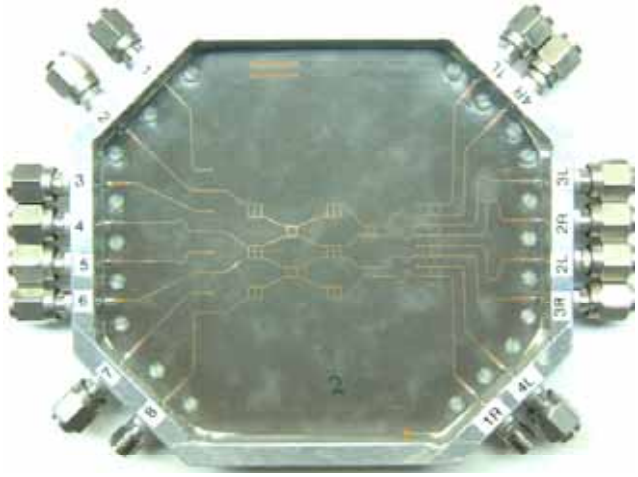

Fig. 15. The Butler matrix as realized. Vertical transitions (on the left) were added at the antenna ports of the bottom layer to bring the signal on top, allowing connector attachment.

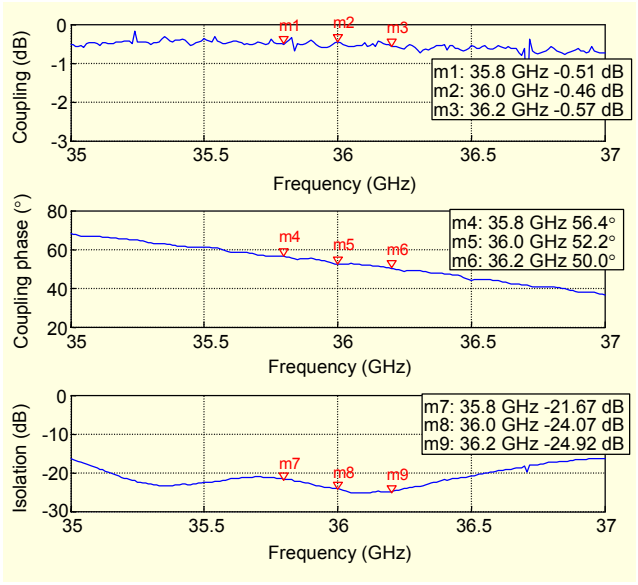

Fig. 16. Measured insertion loss and isolation for the cross-coupler.

3. Vertical Interconnection

Tests of this component were made in a universal test fixture with TRL calibration in-fixture. Since connection was only possible on the top layer, the test circuit was made of two cascaded transitions as shown in Fig. 18. Parameter extraction for a single transition was made by using a proper de-embedding technique based on wave cascading matrixes and a non-linear equation solver.

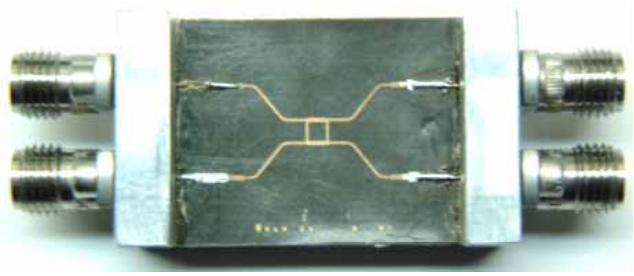

Fig. 17. The quadrature hybrid as realized. Note the rework on port 1, which makes the results irrelevant.

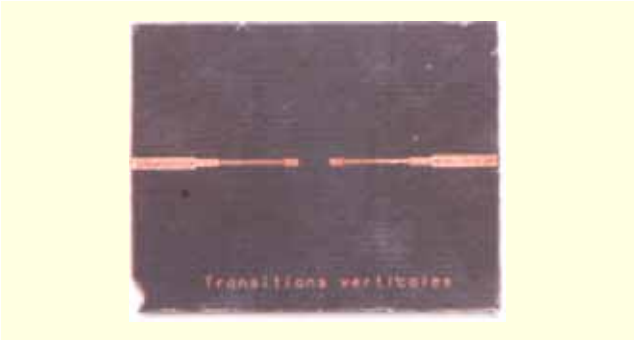

Fig. 18. Realization of the two end-to-end vertical transitions.

An insertion loss of 0.7 dB is achieved experimentally at 36 GHz for a single transition. This result is pretty close to the prediction (0.73dB) obtained by previous simulations shown in Fig. 11, which makes us confident about the modeling process. The measured insertion phase is -27.9° at 36 GHz vs -11.5° simulated. The experimentally-achieved matching is better than the predictions (a return loss lower than -20 dB).

4. Discussion on Measurement Results

The available experimental data for the individual components is close to the simulated results, but relatively small errors were encountered. Unfortunately, the accumulation of these little discrepancies between models and realization makes the whole matrix's performance far from the predictions. The performance in terms of gain and sidelobe level is affected by phase errors, amplitude errors, and insertion losses of the network. This degradation can be observed on the summarized data given in Table 2.

The right beams are more affected by losses, which is essentially because the impedance they present at their inputs is poorly matched to the line impedance Z0. After investigation,

Table 2. Comparative results for the Butler matrix with a linear array of isotropic antenna elements. Spacing between consecutive elements is 4.17 mm and coupling is not considered (see text for description of the parameters).

Parameter	1L/1R	2L/2R	3L/3R	4L/4R	Unit
Ideal					
SLL	-12.8 /-12.8	-12.8/-12.8	-12.8/-12.8	-12.8/-12.8	dB
θ_{max}	-7.2/7.2	-22.0/22.0	-38.7/38.7	-61.0/61.0	○
Gain=directivity	9.0/9.0	9.0/9.0	9.0/9.0	9.0/9.0	dBi
Simulation results: Frequency = 36 GHz					
rms phase error	2.7/2.9	6.7/5.5	5.8/3.8	5.6/3.9	○
rms amplitude error	0.075/.064	0.106/0.05	0.072/0.027	0.062/0.055	-
SLL	-12.5/-12.9	-10.4/-11.2	-11.7/-12.5	-11.3/-11.9	dB
θ_{max}	-7.2/7.0	-22.3/22.3	-38.5/38.3	-61.4/60.8	○
Directivity	9.0/9.0	8.9/9.0	8.9/9.0	9.0/9.0	dBi
Gain	6.2/6.1	5.3/5.7	6.0/5.4	6.0/6.0	dBi
Losses	2.8/2.9	3.6/3.3	2.9/3.6	3.0/3.0	dB
Return loss	-16.1/-17.8	-13.7/-13.2	-23.6/-22.1	-14.2/-14.1	dB
Measured results: Frequency = 36 GHz					
rms phase error	31.6/32.1	23.2/20	19.1/22	30.9/24.9	○
rms amplitude error	0.093/.066	0.1/0.053	0.051/0.092	0.007/0.101	-
SLL	-3.8/-4.0	-6.9/-6.3	-7.6/-8.8	-3.4/-4.0	dB
θ_{max}	-9.5/3.8	-24.8/20.3	-39.6/35.3	-64.8/56.2	○
Directivity	7.7/7.5	8.0/8.3	8.1/8.3	7.1/7.7	dBi
Gain	3.3/-0.8	6.8/3.3	3.8/0.9	3.9/1.3	dBi
Losses	4.4/8.3	1.2/5.0	4.3/7.4	3.2/6.4	dB
Return loss	-10.4/-3.6	-15.3/-10.9	-14.0/-7.0	-22.8/-6.3	dB

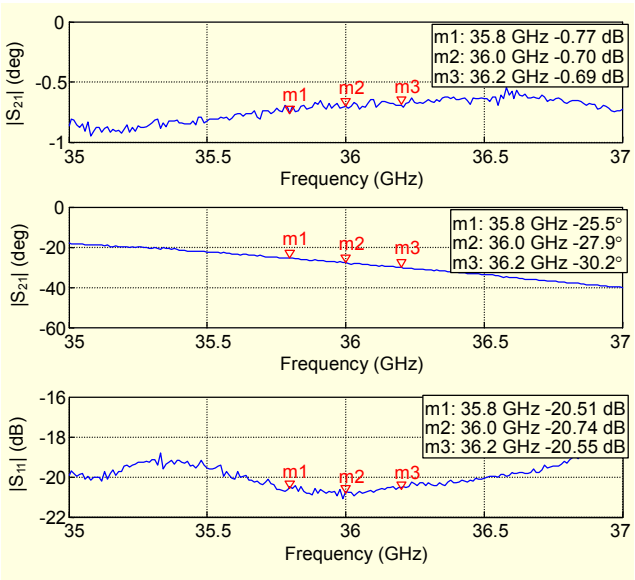

Fig. 19. Measured insertion loss, insertion phase, and return loss for the vertical interconnection.

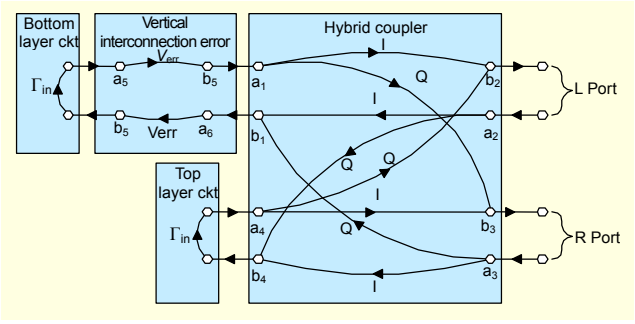

Fig. 20. Simplified signal flow graph of the beam ports used for investigating the return loss variation of the R and L beams.

we can conclude that this is due to the unexpected phase imbalance of the hybrid couplers combined with the phase error introduced by the vertical interconnections.

The relationship between the return losses of the L beams and R beams can be extracted from a simple signal flow graph as shown in Fig. 20. To simplify the analysis, the input and output return losses of the vertical interconnection was set to 0 (S_{11}=S_{22}=0). The return loss for the hybrid coupler was also neglected on all ports (S_{11}=S_{22}=S_{33}=S_{44}=0) and a perfect isolation was assumed (S_{14}=S_{41}=S_{23}=S_{32}=0).

From this representation of the circuit, the reflection coefficient at the L and R beam ports, respectively, can be calculated as follows:

$$\Gamma_L = \frac{b_2}{a_2} = \left(I^2 V_{err}{}^2 + Q^2\right)\Gamma_{in} \tag{6}$$

and

$$\Gamma_R = \frac{b_3}{a_3} = \left(I^2 + Q^2 V_{err}^2\right)\Gamma_{in}\,. \tag{7}$$

The hybrid coupler coefficients S_{21}=S_{12}=S_{34}=S_{43}=I and S_{31}=S_{13}=S_{24}=S_{42}=Q are for the in-phase and quadrature paths, respectively. The term

$$V_{err} = \frac{\text{Measured } S_{21}}{\text{Simulated } S_{21}} \tag{8}$$

is the ratio between measurements and simulations for the vertical interconnection. Finally, Γ_{in} is the reflection coefficient presented by the remaining part of the circuit.

From (6) and (7), it can be shown that the return loss is the same for the L and R beams $\left(\Gamma_L = \Gamma_R\right)$ when there is no error introduced by the vertical interconnection (V_{err}=1). With the error obtained here for the vertical interconnection $\left(V_{err} = 0.03dB\angle -16.4°\right)$ and with a positive phase imbalance for the hybrid, it is easy to show that the input return loss for the R beams degrades significantly. As an example, for a 5 degree imbalance, the R beams have an input return loss of Γ_{in} −8.7 dB , while the L beams have an input return loss of Γ_{in} −14 dB . With this simple demonstration, it is easier to understand the difference between the L and R beams.

PCB manufacturing tolerances in this case were really loose (standard PCB manufacturing facilities were employed). Microscope observation of critical lines and gaps on the realized prototype showed etching errors as high as -30 μm for lines and +16.8 μm for gaps, which can explain why the results are so different. In order to better investigate the effect of theses errors on the performance of such a circuit, a tolerance sensitivity analysis should have been done.

V. Conclusions

In this paper, the feasibility of an 8 × 8 Butler matrix using a multi-layered microstrip assembly in the EHF band has been demonstrated. The vertical interconnection between layers using electromagnetic coupling is a key component of such a structure, and its performance has been measured with satisfying results: 0.7 dB of insertion loss at 36 GHz. The simulation of the whole Butler matrix with isotropic antennas yielded a predicted loss of around 3 dB for the main beam gain of the eight generated beams and a sidelobe level of -10.4 dB for the worst case. In order to better predict the performance of the matrix with antenna elements and coupling, simulations should include the antenna array, of course at the expense of a larger computational task.

To improve the matrix performance, a second iteration of the design should be done including the experimental data for

components like couplers and transitions. Better manufacturing tolerances should be used and a sensitivity analysis should be done. The use of vias should be reconsidered even though their fabrication is critical at these frequencies.

Finally, it appears that these experimental results are among the first of their kind. This circuit is an essential component of a switched beam smart antenna and will be used for this type of application in the close future with antennas and switching network integrated on the same board.

References

[1] M. J. Gans, R. A. Valenzuela, J. H. Winters, and M. J. Carloni, "High Data Rate Indoor Wireless Communications Using Antenna Arrays," *Sixth IEEE Int'l Symp. Personal, Indoor and Mobile Radio Communications*, Toronto, Canada, 1995, pp. 1040–1046.

[2] P. F. Driessen, "Gigabit/s Indoor Wireless Systems with Directional Antennas," *IEEE Transactions on Communications*, vol. 44, Aug.1996, pp. 1034–1043.

[3] J. L. Butler, "Digital, Matrix and Intermediate-Frequency Scanning," *Microwave Scanning Antennas*, R. Hansen, ed., Academic press, New York, vol. 3, 1966, pp. 217–288.

[4] R. De Lillo, "A High Performance 8-Input, 8-Output Butler Matrix Beamforming Network for Ultra-broadband Applications," *IEEE Antennas and Propagation Society Int'l Symp.*, Ann Arbor, MI, USA, vol. 1, 1993, pp. 474–477.

[5] M. Bona, L. Manholm, J. Starski, and B. Svensson, "Low-Loss Compact Butler Matrix for a Microstrip Antenna," *IEEE Transactions on Microwave Theory and Techniques*, vol. 50, Sept. 2002, pp. 2069–2075.

[6] T. Denidni and T. Libar, "Experimental Investigation of a Microstrip Planar Feeding Network for a Switched-Beam Antenna Array," *Antennas and Propagation Society Int'l Symp.*, vol. 1, June 2002, pp. 130–133.

[7] R. C. Hansen, *Phased Array Antennas,* Wiley, New York, 1998.

[8] J. Reed and G. Wheeler, "A Method of Analysis of Symmetrical Four-Port Networks," *IRE Transactions on Microwave Theory and Techniques*, vol. 4, Oct. 1956, pp. 246– 252.

[9] D. M. Pozar, *Microwave engineering,* Wiley, 2nd ed., New York, 1998.

[10] J. P. Kim and W. S. Park, "An Improved Network Modeling of Slot-Coupled Microstrip Lines," *IEEE Transactions on Microwave Theory and Techniques*, vol. 46, Oct. 1998, pp. 1484–1491.

[11] L. Zhu and K. Wu, "Ultrabroad-Band Vertical Transition for Multilayer Integrated Circuits," *IEEE Microwave and Guided Wave Letters*, vol. 9, Nov. 1999, pp. 453–455.

[12] C. Chen, M.-J. Tsai, and N. Alexopoulos, "Optimization of Aperture Transitions for Multiport Microstrip Circuits," *IEEE Transactions on Microwave Theory and Techniques*, vol. 44, Dec. 1996, pp. 2457–2465.

[13] C. Chen, M.-J. Tsai, and N. Alexopoulos, "Mutual Coupling between Microstrips through a Printed Aperture of Arbitrary Shape in Multilayered Media," *IEEE Microwave and Guided Wave Letters*, vol. 6, , May 1996, pp. 202–204.

Jean-Sébastien Néron received the BSc degree in electrical engineering from École de Technologie Supérieure (ETS), Montréal, Canada in 2000 and the MSc degree in electrical engineering from Laval University, Québec, Canada in 2005. He is currently working for the PhD degree at the Electrical and Computer Engineering department at Laval University, Québec, Canada on the design and realization of a wideband millimetre-wave smart antenna. He was granted the R.A. Fessenden scholarship from the Communications Research Center for 2002 and 2003 and the Canadian Wireless Telecommunications Association prestige scholarship in 2000, 2001, and 2003. He acquired industrial experience in R&D departments, especially on RF Modems, RF measurements and characterization, and embedded systems design, at Marconi Canada, CAE Electronics, and ABL Canada. Inc. His research interests include planar antennas, microwave circuits, and channel characterization at millimetre-wave frequencies.

Gilles-Y. Delisle is Vice-President Research at the International Institute of Telecommunications in Montréal, Canada since July 2004. Previously, he was Director and Professor at the School of Information Technology and Engineering at the University of Ottawa from 2002 to 2004 and he has been a Professor of Electrical and Computer Engineering at Laval University, Québec, Canada, from 1973 to 2001. He is involved in research work in intelligent antenna array, radar cross-section measurements and analytical predictions, mobile radio-channel propagation modeling, personal communications, advanced wireless systems and industrial realization of telecommunications equipment. He is a member of the Order of Engineers of the Province of Québec and Professional engineers of Ontario, Past-President of the Canadian Engineering Accreditation Board, Member of the Canadian Academy of Engineering, Past Canadian President of URSI, Past President of *ACFAS* (*Association Canadienne Francaise pour l'Avancement des Sciences*) and a Fellow of the Institute of Electrical and Electronics Engineers(IEEE), of the Canadian Engineering Institute, of the Canadian Academy of Engineering and of the Institution of Electrical Engineers (IEE). He has supervised the work of over a hundred graduate and post-graduate students over the last 32 years.